MICHIGAN STATE
UNIVERSITY

National Superconducting Cyclotron Laboratory

ISOTOPIC SCALING IN NUCLEAR REACTIONS

M.B. TSANG, W.A. FRIEDMAN, C.K. GELBKE, W.G. LYNCH, G. VERDE, H. XU

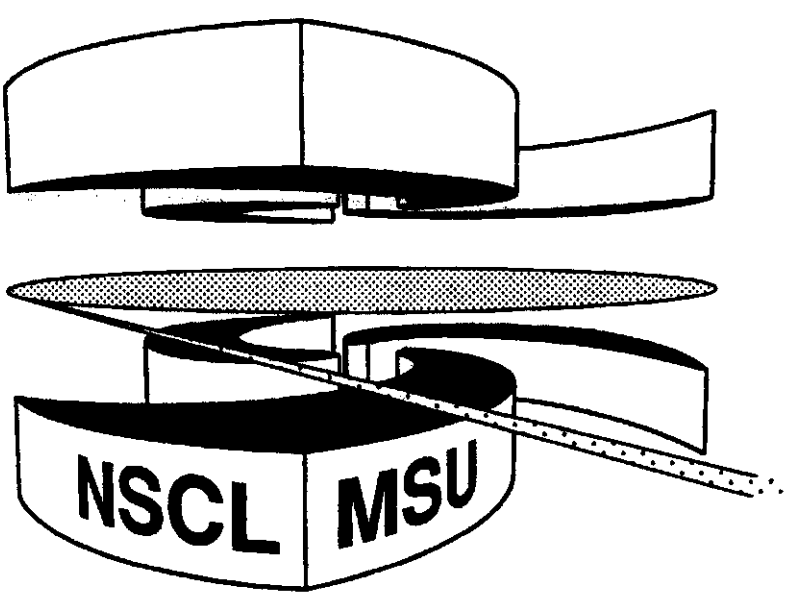

MSUCL-1165 **JULY 2000**

Isotopic Scaling in Nuclear Reactions

M.B. Tsang[1], W.A. Friedman', C.K. Gelbke', W.G. Lynch', G. Verde', H. Xu[1]

[1] National Superconducting Cyclotron Laboratory and Department of Physics and Astronomy, Michigan State University, East Lansing MI 48824,

[2] Department of Physics, University of Wisconsin, Madison, WI 53706

Abstract

A scaling between isotopic distributions for elements with $Z \leq 8$ has been observed which allows a transparent characterization of the dependence of such distributions on the overall isospin of the system. For the cases investigated, this scaling is not very sensitive to secondary decays and applies to a broad range of statistical production mechanism including evaporation, strongly damped binary collision, and multifragmentation. The origins of this scaling behavior for the various reaction mechanisms are explained and the implications for future research are discussed.

The availability of high intensity radioactive beams facilitates the exploration of the isospin degree of freedom in nuclear reactions. The isotopic degree of freedom is especially important for understanding the behavior of the charge symmetry term of the nuclear equation-of-state[1-3], for obtaining information about charge equilibration[4-6], and for providing stringent tests for reaction models. Understanding the connection between the entrance channel isospin and the isotopic distribution of reaction products is also important for optimizing production of rare isotopes far from stability. Large solid angle measurements of isotopic yields that can provide insight into such issues are rare. Nonetheless, recent measurements have revealed systematic isospin dependencies [7] that now appear to be manifested in a variety of nuclear reactions over a wide range of incident energies.

To illustrate how such isotopic yields may be systematized, we examine the dependence of the isotopic yields within the grand-canonical ensemble. While this approach is not strictly valid for finite nuclear systems, it offers the advantage of transparent analytical formulae. In this approach the isotopic yields are governed by both the neutron and proton chemical potentials, μ_n and μ_p and the temperature T, plus the individual binding energies, B(N,Z), of the various isotopes [8,9]:

$$Y(N,Z) = F(N,Z,T) \cdot \exp(B(N,Z)/T) \cdot \exp(N\,\mu_n/T + Z\,\mu_p/T) \qquad (1)$$

The factor $F(N,Z,T)$ includes spin degeneracies and information about the secondary decay from both particle stable and particle unstable states to the final ground state yields. A precise global description of experimental isotope distributions is difficult due, in part, to the complexity of describing the excitation and decay reaction products from states far above the energy threshold for particle emission[10-12]. Similarly, the accurate prediction of $F(N,Z,T)$ is difficult due to a lack of comprehensive energy, spin and branching ratio information about many relevant levels that contribute to these decays[10-12]. It has been

shown that some of these difficulties can be minimized by assuming that the influence of secondary decay on the yield of a specific isotope is similar for two different systems labeled 1 and 2 that have same temperature but different isospins, i.e. $F_1(N,Z,T) \approx F_2(N,Z,T)$ [7]. In this case, the relative isotope yield ratio, $R_{21}(N,Z)$, depends on only three parameters [7]:

$$R_{21}(N,Z) = Y_2(N,Z)/Y_1(N,Z) = C \cdot \exp(N \cdot \alpha + Z \cdot \beta) \quad (2)$$

where $\alpha = \Delta\mu_n/T$ and $\beta = \Delta\mu_p/T$ reflect the differences between the neutron and proton chemical potentials for the two reactions and C is an overall normalization constant. The parameters α, β and C are obtained by fitting R_{21}. To simplify the expressions used throughout this article, we define differences between the observables for the two systems as $\Delta X = X_2 - X_1$, e.g. $\Delta\mu_p = \mu_{p,2} - \mu_{p,1}$. We have also chosen the system in the numerator to be more neutron-rich than the one in the denominator, i.e. $N_2/Z_2 > N_1/Z_1$. This definition differs from that of Ref. [13-15] where the inverse ratios, $R_{12}(N,Z)$ have been used.

The accuracy of this representation can be very compactly displayed by constructing a scaled isotopic ratio, $S(\beta) = R_{21} \cdot \exp(-\beta\, Z)$ as a function of N. Where this parameterization is accurate and the best fit value of β is chosen, values for $S(\beta)$ of all elements lie along a straight line on a semi-log plot. We refer to this trend as *isotopic scaling*. The data points plotted next to the label "multifragmentation" in Figure 1 denote values for $S(\beta)$ extracted from ratios of isotopically resolved differential multiplicities extracted from multifragmentation events in central $^{124}Sn + ^{124}Sn$ and $^{112}Sn + ^{112}Sn$ collisions[7]. The scaled isotope ratios for fragments with $3 \leq Z \leq 8$ lying along a single line, is consistent with Eq. 2 and the well known success of equilibrium parameterizations for multifragmentation [16]. More surprisingly, the isotopic scaling is observed for other reactions shown in Figure 1: strongly damped binary collisions (^{16}O induced reactions on two targets ^{232}Th and ^{197}Au) [17] and evaporative compound nuclear decay ($^4He + ^{116}Sn$ and $^4He + ^{124}Sn$ collisions)[14], for which

Grand-Canonical Ensemble approaches would appear to have little relevance. Why isotopic scaling is also observed in these cases is examined below.

An examination of strongly damped collisions reveals that isotopic scaling is reasonably well respected at low incident energies ($E/A < 10MeV$) and at relatively backward angles i.e. when equilibrium is established between the orbiting projectile and target. In such cases, the isotopic yields follow the "Q_{gg}-systematics"[17,18], in which the primary isotope yield of the projectile-like fragment depends primarily on the Q-value of the mass transfer and can be approximated by

$$Y(N,Z) \propto \exp((M_P + M_T - M'_P - M'_T)/T) \tag{3}$$

where M_P and M_T are the initial projectile and target masses, and M'_P and M'_T are the final masses of the projectile- and target-like fragment. Here, T has a natural interpretation as the temperature, but is not always assumed to be so. Using this expression, charge and mass conservation, and expressing explicitly only the terms that depend on N and Z, one can write R_{21} as

$$R_{21}(N,Z) \propto \exp[(BE(N_2 - N, Z_2 - Z) - BE(N_1 - N, Z_1 - Z))/T], \tag{4}$$

where Z_i and N_i are the total proton and neutron number of reaction i. BE is the binding energy of a nucleus. Expanding the binding energies in Taylor series, one obtains an expression of the form

$$BE(N_2-N,Z_2-Z)-BE(N_1-N,Z_1-Z) \approx -\Delta s_p \cdot Z - \Delta s_n \cdot N + c \cdot Z^2 + d \cdot N^2 + e \cdot ZN, \tag{5}$$

where Δs_p and Δs_n are the differences of the neutron and proton separation energies for the two compound systems. Evaluating Eq. 5 within the context of a liquid drop expansion, one

finds that the second order terms are of order (1/A), where A the mass number, relative to the first order terms. The leading order term in equation 4 becomes

$$R_{21} \propto \exp[(-\Delta s_n \cdot N - \Delta s_p \cdot Z)/T]. \tag{6}$$

Comparison of Eqs. 2 and 6 reveals that the difference in the average separation energies plays a corresponding role to the difference in chemical potentials in the grand canonical expression, an intriguing result when one considers that $\mu \approx -s$ in the low temperature limit[12]. From Eq. 5, one expects that Eq. 6 will become less accurate and eventually break down leading to a failure in isotopic scaling when the range of fragment masses considered becomes large. More detailed examination suggests that one may also expect the breakdown of this scaling trend for target and projectile far from the valley of stability.

Next we consider the yields from higher energy reactions involving the formation of a composite system and the subsequent decay via evaporation of different isotopes. The scaling behavior for fragments detected at backward laboratory angles ($\theta = 160^o$) in $^4He + ^{116}Sn$ and $^4He + ^{124}Sn$ collisions at $E/A = 50MeV$ [14] is illustrated in Figure 1, next to the label "evaporation". Scaling is not respected in these reactions at forward angles where contributions from pre-equilibrium processes become significant [14].

To explore the factors which govern the evaporation rates of different species that contribute to the evaporation systematics, we utilize the formalism of Friedman and Lynch [19] which provides statistical decay rates derived from detailed balance as in the Weisskopf model [20]. When the relative rates are dominated by emission within a particular window of source-mass or source-temperature, the relative yields are directly related to the instantaneous rates

$$dn(N,Z)/dt \propto T^2 \cdot \exp(-V_c/T + N \cdot f_n^*/T + Z \cdot f_p^*/T - B/T) \tag{7}$$

where V_c gives the Coulomb barrier, and the terms f_n^* (f_p^*) represent the excitation contribu-

tion to the free energy per neutron (proton). These factors are often modeled by the excited Fermi gas wherein they attain values determined by the temperature and density of the neutron (proton) distribution. The factor $B = BE(N_i, Z_i) - BE(N_i - N, Z_i - Z) - BE(N, Z)$ reflects the separation energy associated with the removal of the isotope from the parent nucleus, here denoted by the subscript "i".

If one calculates R_{21} using yields from two systems, and if one adopts the approximations for the binding energy differences between parent and daughter nuclei utilized in Eq. 6, one obtains:

$$R_{21}(N, Z) \propto exp[\{(-\Delta s_n + \Delta f_n^*) \cdot N + (-\Delta s_p + \Delta f_p^* + e\Delta\Phi(Z_i - Z)) \cdot Z\}/T] \quad (8)$$

where $\Phi(Z)$ is the electrostatic potential at the surface of a nucleus with neutron and proton number N and Z. The sum of the separation energies, free excitation energies and electrostatic potentials play the same roles as chemical potentials in Eq. 2. As the second order term from the electrostatic potential is small for the decay of large nuclei, all factors in the exponent are proportional to either N or Z. Eq. 8 suggests that isotopic scaling can be expected for evaporation of nuclei with masses small in comparison to the total mass.

In a similar manner, relative isotope ratios predicted for multifragmentation processes by the Expanding Evaporating Source (EES) model [21] will also display isotopic scaling. This latter model utilizes a formula for the particle emission rates which is formally identical to that of Eq. 8 but assumes values for the separation, Coulomb, and free energies, B, V_c and f^* that differ from those in Eq. 7 principally because the residue may expand to sub-saturation density. In this circumstance, the separation energies may vanish or become negative, enhancing the emission rate of fragments with $3 \leq Z \leq 20$. As in the case of pure evaporation theory, all factors in the exponent are proportional to either N or Z.

Thus in all four models, compound nuclear evaporation, strongly damped binary col-

lisions, equilibrium multifragmentation, and the time dependent EES multifragmentation model[21], isotopic scaling is expected because the logarithm of the relative rates can be expanded to first order in N and Z . At low excitation energies, the differences in the neutron and proton separation energies for the two systems are major factors in all expressions. For systems of comparable mass but very different N/Z ratio, the volume, surface, and Coulomb contributions to the separation energy largely cancel. The most important contribution to the differences in the neutron and proton separation energies in R_{21} comes from the symmetry term in the semi-empirical (liquid-drop) mass formula. In the EES model, this symmetry term must be extrapolated to sub-saturation density as the system expands; a measurement of R_{21} can thereby probe the density dependence of the symmetry energy [22]. Recent SMM model calculations [12] indicate that μ_n and s_n are closely related ($\mu_n \approx -s_n + f_n^*$) for $0 \leq T \leq 3MeV$, where the decay configurations are mainly binary, but the connection between μ_n and s_n becomes increasingly weak as the role of multifragment decay configurations become important. For multifragment decays in the equilibrium limit, the chemical potentials carry the information determining the relative N/Z ratios of the free nucleons and light particles and how this differs from the N/Z ratio of more strongly bound fragments. If the fragments expand at high temperature, the chemical potentials will reflect the density dependence of their symmetry energies as well [21,23].

The utilization of single separation energies or chemical potentials in Eqs. 1-8 is an approximation that will break down when the range of fragment charges and masses included in the scaling plot becomes larger. The non-linear terms in the exponent come both from the symmetry energy of the remaining system and from Coulomb potential terms. As more detailed data over a broader range of nuclei become available, it may be interesting to expand the exponents in Eqs. 1-8 to second order in N and Z and explore the emerging systematics. Many micro-canonical equivalents to the formalism for multifragmentation represented by Eq. 1 have Coulomb terms that are explicitly quadratic, density dependent, and opposite in

sign to the term V_c in Eq. 8.

The systematics described by Eq. 2 rely on the emission mechanism for the fragments in each reaction being described statistically with some common effective temperature and that distortions from secondary decays cancel[7, 13-15]. However, one should note with caution that exhibition of the systematic trends does not imply that both reacting systems proceed with the same reaction mechanism. The data labeled as "mixed" in Fig. 1 demonstrate this point. The isotopic yields of fragments produced in central $Au + Au$ multifragmentation process at $E/A = 35MeV$ [24] can be related via isotopic scaling to those produced in lower multiplicity evaporation process produced in $Xe + Cu$ reactions at $E/A = 30MeV$[25]. As the emission mechanisms in the two reactions differ significantly, the parameters α and β will reflect a mixture of factors from the evaporation and multifragmentation models, evaluated at slightly different temperatures for the two reactions. Nothing from the systematics itself reveals this complexity of interpretation. In order to draw correct conclusions from isotopic measurements, it is therefore absolutely essential to obtain additional experimental information that elucidates the underlying reaction mechanism.

In summary, we have observed a scaling between isotopic distributions which allows a transparent characterization of the dependence of such distributions on the overall isospin of the system. This scaling applies to a broad range of statistical production mechanisms including evaporation, strongly damped binary collision, and multifragmentation. We have shown how this systematics can be explained by the theories most frequently applied to such processes and suggested that higher order terms may lead to deviation when the study is extended over much wider ranges of charge or neutron number.

This work was supported by the National Science Foundation under Grant Nos. PHY-95-28844 and PHY-96-05140.

Figure Caption:

Figure 1: The scaled isotopic ratio, $S(\beta)$ is plotted as a function of N using the best

fit value of β obtained from fitting isotopes with $Z \geq 3$. The data points plotted next to the label "multifragmentation" in Figure 1 denote $S(\beta)$ extracted from multifragmentation events in central $^{124}Sn + ^{124}Sn$ and $^{112}Sn + ^{112}Sn$ collisions[7] with $\beta = -0.40$, $\alpha = 0.36$. The data labeled as "mixed" are $S(\beta)$ constructed from isotope yields produced in central $Au + Au$ multifragmentation events [24] and evaporation events in $Xe + Cu$ [25] reactions with $\beta = -0.27$, $\alpha = 0.41$. The scaling behavior for evaporation process is illustrated by the reactions $^{4}He + ^{116}Sn$ and $^{4}He + ^{124}Sn$ [14] plotted next to the label "evaporation" with $\beta = -0.82$, $\alpha = 0.60$. Systematics of the strongly damped binary collisions is represented by the data of ^{16}O induced reactions on two targets ^{232}Th and ^{197}Au [17] plotted next to the label "deeply inelastic" with $\beta = -1.1$, $\alpha = 0.74$.

References:

1. Bao-An Li et al., Phys. Rev. Lett. 78, 1644 (1997).

2. I. Bombaci, et al., Phys. Rep. 242, 165 (1994).

3. J.M. Lattimer and M. Prakash, Ap. J. (in press).

4. R. Laforest et al., Phys. Rev. C59 2567 (1999) and refs. therein.

5. R. Wada et. al., Phys. Rev. Lett. 58, 1829 (1987).

6. W.U. Schroder and U.J. Huizenga, Treatise on heavy Ion Science, Ed. D.A. Bromley (Plenum Press, 1984) and references therein.

7. H. Xu et al., Phys. Rev. Lett. (in press).

8. J. Randrup and S.E. Koonin, Nucl. Phys. A 356, 223 (1981);

9. S. Albergo et al., Nuovo Cimento A 89, 1 (1985).

10. T.K. Nayak et al., Phys. Rev. C 45, 132 (1992).

11. H. Xi et al., Phys. Rev. C 59, 1567 (1999)

12. S. R. Souza et al., NSCL preprint MSUCL-1152 and to be published

13. O.V. Lozhkin et al., Phy. Rev. C 46, 1996 (1992) and references therein.

14. J. Brzychczyk et al., Phys. Rev. C47, 1553 (1993).

15. Y. Murin et al., Europhys. Lett. 34, 337 (1996); Y. Murin et al., Physca Scripta 56, 137 (1997).

16. M. D'Agostino et al., Phys. Lett. B 371, 175 (1996); B.A. Li et al., Phys.Lett.B303, 225 (1993); A.S. Botvina et al., Nucl. Phys. A 584, 737 (1995).

17. V.V. Volkov, Phys. Rep. 44, 93, (1978).

18. C.K. Gelbke et. al., Phys. Rep. 42, 311 (1978)

19. W. Friedman and W. Lynch, Phys. Rev. C 28, 950 (1983).

20. V. Weisskopf, Phys. Rev, 52, 295 (1937).

21. W.A. Friedman, Phys. Rev. Lett. 60, (1988) 2125; and Phys. Rev. C42, 667 (1990).

22. Note: $f^*(T/\epsilon_f)/T$ remains roughly constant during expansion.

23. H. Müller and B. D. Serot, Phys. Rev. C 52, 2072 (1995).

24. M.J. Huang et. al., Phys. Rev. Lett. 78, 1648 (1997)

25. H. Xi et al., Phys. Rev. C 57, R462 (1998)

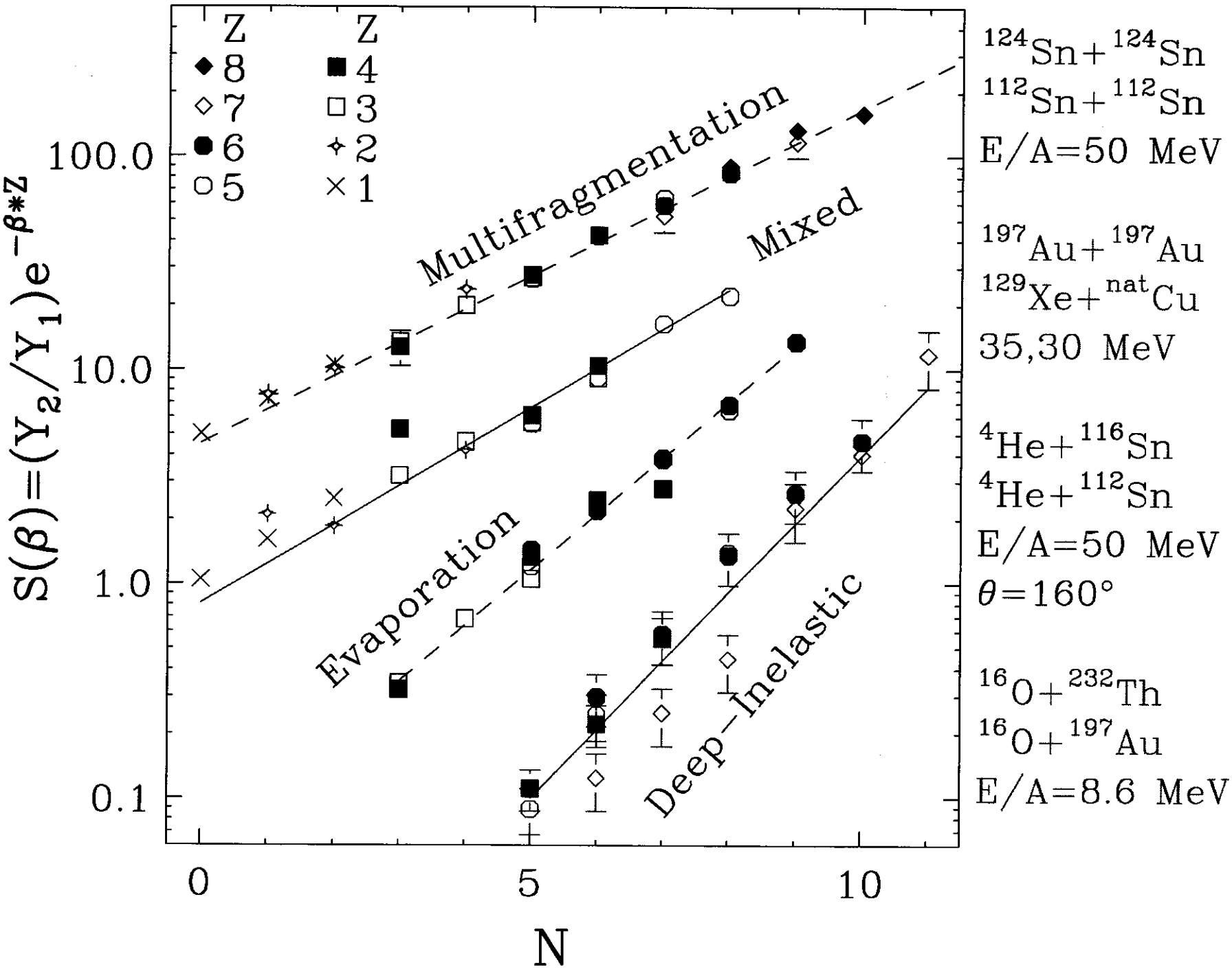
Z
8
7
6
5
Z
4
3
2
1
Multifragmentation
Mixed
Evaporation
Deep−Inelastic
$S(\beta)=(Y_2/Y_1)e^{-\beta*Z}$
100.0
10.0
1.0
0.1
0
5
10
N
$^{124}Sn+^{124}Sn$
$^{112}Sn+^{112}Sn$
E/A=50 MeV
$^{197}Au+^{197}Au$
$^{129}Xe+^{nat}Cu$
35,30 MeV
$^{4}He+^{116}Sn$
$^{4}He+^{112}Sn$
E/A=50 MeV
θ=160°
$^{16}O+^{232}Th$
$^{16}O+^{197}Au$
E/A=8.6 MeV